Adhesive hard-sphere colloidal dispersions: Fractal structures and fractal growth in silica dispersions

P. W. Rouw and C. G. de Kruif
Van 't Hoff Laboratory, University of Utrecht, Padualaan 8, de Uithof, 3584 CH Utrecht, The Netherlands
(Received 19 July 1988)

Silica particles coated with octadecyl chains and dispersed in linear alkanes (dodecane and higher alkanes) show gelation upon cooling. The structure of these gels can be characterized in terms of a fractal dimension $d_f=2.1$. Aggregation and gelation at temperatures just below the cloud point (the temperature at which phase transition occurs) have been studied by light scattering and are described in terms of the finite linear cluster size (cluster radius) ξ of the growing fractal. This size is found to increase linearly with time. The influence on d_f of quench temperature, volume fraction, particle size, and solvent type is discussed.

I. INTRODUCTION

In the last few years there has been growing interest in the field of fractal structures. Since the formulation of the fractal concept by Mandelbrot[1] there have been numerous publications in which random structures of aggregates and gels are described in terms of this concept. In dendritic growth where a single particle (monomer) sticks to a central cluster, one can see quite clearly from photographs that the total mass contained in a spherical shell diminishes with increasing distance from the center of the cluster. For a homogeneous sphere, mass is proportional to R^3. The mass of a fractal cluster contained in a sphere with radius R is proportional to R^{d_f}, where d_f is smaller than 3 in three dimensions. However, the fractal concept cannot be applied at all length scales in a collidal cluster. There is usually a lower cutoff length which is set by the size of the monomeric unit, i.e., molecules or (colloidal) particles. The upper cutoff length is set by the "average" size of the clusters which may be restricted by the size of the container. Provided upper and lower cutoff lengths are separated by several orders of magnitude, the fractal concept can be used for length scales in between. For small values of d_f the average density of a cluster is small. The power-law relation between mass and length scale (radius) is characteristic for a fractal cluster. A good example of the scale invariance characteristic for fractals is found in the study of aggregation of gold sols by Weitz and Huang.[2] It is seen that the shape of the clusters is not affected by the magnification factor, i.e., the clusters are scale invariant.

Soon afterwards, models were developed which relate the fractal morphology to the mechanism by which the structure is formed.[3–6] Computer simulations are widely used to set up and test these models.[7] Usually three main categories of mechanisms are distinguished.

In the Witten-Sander model or *diffusion-limited aggregation* (DLA) the fractal dimension, relating the mass within a certain radius to this radius [$M(r)\sim r^{d_f}$], is found to be about 2.52 (Ref. 8) in three dimensions. The open structure is due to the fact that monomers cannot enter the interior of the growing fractal since they stick irreversibly to this structure upon contact. In this model only a single cluster grows, which is not very realistic. However, Sinha *et al.*[9] studied compacted vapor-phase aggregates of silica by means of small-angle neutron scattering. From these experiments they could deduce a fractal dimension of 2.52 which is close to the value found for diffusion-limited aggregation.

In *cluster-cluster aggregation* one allows more than one cluster to form; growth is due not only to monomer addition but also to the sticking of the clusters to each other. One obtains a fractal dimension of 1.75–1.80. This cluster-cluster aggregation is still diffusion-limited, i.e., there is a high sticking probability. The lower fractal dimension indicates that this mechanism leads to a much more open structure. Weitz and Oliveria[10] performed transmission electron microscopy measurements on aggregating gold sols and found $d_f=1.75$. Almost the same value (1.77) was found by Aubert and Cannell[11] who studied silica under rapid aggregation conditions. These values are in perfect agreement with the cluster-cluster model. The relation between cluster radius and time is found to be[12]

$$\xi(t)\sim t^{[1+d_f(1-\alpha)-d]^{-1}}, \quad v_i\sim i^{\alpha},$$

where v_i is the velocity of a cluster consisting of i particles (monomers).

Chemically-limited aggregation (CLA) occurs when there is a low sticking probability. The origin of the low sticking probability is often of a chemical nature and therefore aggregation is said to be chemically limited. Clusters formed by this mechanism are more dense and computer simulations show a fractal dimension of 2.11 (Ref. 6). Schaefer *et al.*[13] studied colloidal silica aggregates using both light scattering and x-ray scattering. From these experiments they obtained a value of $d_f=2.1$. A value for $d_f=2.08$ was found by Aubert and Cannell[11] who studied slow aggregation of silica by changing the *p*H and by adding salt. Aggregation kinetics has not been studied very much theoretically. Recent-

ly, however, Ball *et al.* attempted to model CLA.[14] Experiments[15,16] and theory indicate that cluster radius increases exponentially with time.

Computer simulation can be used to model many other types of mechanisms. In recent research, models have been devised in which the sticking conditions are modified. Meakin and Jullien[17] studied effects of particle rearrangement after sticking due to deformation of the clusters. Reversibility in the aggregation process can also be obtained by the introduction of a finite lifetime of the bonds between the particles and by the introduction of a probability of bond formation p (being smaller than 1).[18,19] For these models two time scales are distinguished. At early times the number of bonds that are formed is much larger than the number of bonds that are broken. This stage corresponds to irreversible aggregation. For long times a dynamic equilibrium is reached between the formation and breaking of bonds. This stage corresponds to reversible aggregation and computer simulation shows that $d_f = 2.03 \pm 0.05$.

As already indicated, there are several ways of determining the fractal dimension of gels and aggregates. Weitz and Huang[2] found the fractal dimension from electron micrographs by determining the mass of the clusters as a function of their radius $M(r) \sim r^{d_f}$. Scattering techniques are often used to characterize fractal structures. One can use static light scattering[13] (SLS), small-angle x-ray scattering,[20] and small-angle neutron scattering.[21] A clear review paper on scattering from fractals has been written by Martin and Hurd.[22] Turbidity measurements[23] and dynamic light scattering[24,25] have also been used recently to determine fractal dimensions.

Many authors have reported on aggregation in colloidal systems. Weitz and Huang[2] studied the kinetics of aggregation of gold colloids by adding pyridine and found a fractal dimension of 1.75. Cluster radius was found to increase as $t^{2.6}$ for short times and as $t^{0.5}$ for long times. Schaefer *et al.*[13] studied the aggregation of charged silica particles in solutions by the addition of salt. They determine the fractal dimension both by light and x-ray scattering and found a value of 2.12. Freltoft *et al.*[21] performed small-angle neutron scattering measurements on silica powders and found a fractal dimension of 2.61 for the dry samples and 2.34 for the water-suspended samples. Schaefer and Keefer[20] studied polymerization of charged silica under different conditions. They found different fractal dimensions depending on the particular preparation method used. Fractal dimensions ranged from 1.9 to 2.8. Pusey and Rarity[24] determined the fractal dimension of polystyrene aggregates by dynamic and static light scattering. Aggregation was induced by the addition of salt. They found $d_f = 2.08$. Using dynamic light scattering, Martin[25] studied dilute aggregates of colloidal silica and found $d_f = 2.05$, which is in agreement with previous results. In his study aggregate growth was found to be exponential with time.

Fractal properties of colloidal aggregates are usually studied in charge-stabilized systems and aggregation is induced by the addition of salt or by changing the pH. In most cases particle interaction is not well controlled and can be changed only from (highly) repulsive to (highly) attractive.

We, on the other hand, studied silica particles coated with octadecyl chains and dispersed in n-alkanes. Interaction between the particles is governed by the free energy of the mixing of chains and solvent.[26] In these sterically stabilized dispersions attraction between the particles can be induced by reducing the solvent quality. Solvent quality can be changed by changing the temperature.[27–29] Attraction between the particles then leads to phase separation of the gas-liquid type or to gelation. Interaction between the particles in our system can be tuned by fixing the temperature of the dispersion. At high temperatures interaction is repulsive but at low temperatures attraction between the particles occurs. One can observe this change in interaction by measuring the turbidity as a function of temperature. At a certain temperature called the cloud point, there is an abrupt increase in turbidity (see Appendix A). Here attraction between the particles is sufficient to induce a phase transition. For silica dispersions in long n-alkanes (C_{12}, C_{14}, and C_{16}) cooling just below the cloud point leads to a phase separation. Depending on volume fraction and quench depth the systems show aggregation (sample still flows) or gelation (sample is rigid). Also, there is a gradual transition from aggregates to gel if the system is kept at the quench temperature long enough. Light scattering from the aggregated system or gel phase is similar; therefore, we do not make a sharp distinction between them. Gelation is reversible, i.e., raising the temperature restores the initial (monomer) situation. No sign of permanent clusters is observed in the reheated solution.

Aggregation and gelation in silica dispersions in these long n-alkanes can thus be achieved by suddenly lowering the temperature to below the cloud point. In this paper we are concerned with the structure of these aggregates and gels. We will study the influence of quench temperature on d_f. The influence that particle radius, volume fraction, and the kind of solvent have on the fractal dimension is examined. Aggregation kinetics is studied too. One would expect aggregation to be diffusion controlled if the solvent quality is so low that already a few particle collisions lead to sticking, whereas it will be reaction controlled if there is not a strong attraction between the particles and many collisions are necessary for sticking. Since attraction between the particles can be influenced by temperature, there may be a crossover between the two mechanisms going from high to low temperatures. It turns out that at the temperatures studied the clustering kinetics must be described by a reaction-limited process. We analyzed the fractal nature of the aggregates and gels using light scattering.

II. THEORETICAL BACKGROUND

A quantitative description of the mass distribution in a gas or a liquid, as well as inside a cluster, is given by the Van Hove distribution function $G(r)$ (Ref. 30)

$$G(r) = \frac{\langle \rho(0)\rho(r) \rangle}{\rho} , \tag{1}$$

where $\rho(r)$ is a particle density (δ) function and ρ is the average density. The angular brackets indicate an ensemble average over all positions in the cluster and over all orientations. $G(r)$ is related to the radial distribution function $g(r)$ by

$$G(r)=\delta(r)+\rho g(r) , \tag{2}$$

where $\delta(r)$ is the "self-correlation." For a fractal the definition of $G(r)$ must be treated with caution since one has to avoid edge effects. It was shown by Martin and Hurd[22] that scale invariance of the fractal structure implies a particular form of $G(r)$ for these systems. Since the form of $G(r)$ must be insensitive to a magnification factor m, we can formally write

$$G(mr)=m^{-\eta}G(r) .$$

Taking $m=1/r$ results in

$$G(r)=G(1)/r^{\eta} .$$

The mass within a fractal structure is related to $G(r)$;[31]

$$M(\xi)=\int_0^{\xi}G(r)d^3r\sim\int_0^{\xi}r^2G(r)dr\sim\xi^{3-\eta} ,$$

where ξ is the radius of the fractal. Since for fractal structures we have $M(\xi)\sim\xi^{d_f}$, it is clear that $\eta=3-d_f$; thus

$$G(r)=G(1)r^{-\eta}\sim r^{d_f-3} . \tag{3}$$

Consider a suspension of fractal clusters consisting of aggregated monomer particles. We assume that the number density of clusters is so low that there is no correlation between the centers of the clusters. The intensity of the scattered light per unit volume of the sample $R(K)$ can be expressed as

$$R(K)=\kappa c M_m P(K)S(K) . \tag{4}$$

κ is an optical constant that does not concern us here, c is the weight concentration of monomers in the suspension, and M_m is the molar mass of the monomers. K is the wave vector

$$K=\frac{4\pi n}{\lambda_0}\sin(\theta/2) ,$$

where n is the refractive index of the suspension, λ_0 is the wavelength of the light in vacuum, and θ is the scattering angle. The form factor $P(K)$ accounts for the interference of light scattered from different parts within the monomer particle. The structure factor $S(K)$ accounts for interference of light from the different monomers inside the fractal cluster. The light scattering intensity is proportional to the structure factor $S(K)$ which is the Fourier transform of $G(r)-\rho$.[30] For an infinite fractal cluster consisting of infinitesimal monomers, Eq. (3) holds. One finds

$$\begin{aligned}S(K)&=4\pi\int_0^{\infty}[G(r)-\rho]\frac{\sin(Kr)}{Kr}r^2dr\\&=4\pi K^{-d_f}\int_0^{\infty}[(Kr)^{d_f-3}]\frac{\sin(Kr)}{Kr}\\&\quad\times(Kr)^2d(Kr)\\&\quad-4\pi\rho\int_0^{\infty}\frac{\sin(Kr)}{Kr}r^2dr .\end{aligned} \tag{5}$$

Since the last integral vanishes for $K\neq0$ it follows that

$$S(K)=AK^{-d_f} .$$

This equation shows scaling of the structure factor and thus, since $P(K)=1$, also of the scattered intensity with wave vector. Thus measurement of the scattered intensity as a function of wave vector provides a way of determining the fractal dimension of the aggregate.

In practice one always deals with a finite cluster radius ξ and a finite size of the monomers r_0. This causes a breakdown of the power law for the structure factor as a function of wave vector at high values of K since length scales of the order of the size of the monomers are probed. At small K, length scales of the order of the radius of the fractal cluster are probed and scaling no longer holds. Figure 1 shows the different K regions. To account for the finite size of the clusters Freltoft *et al.*[21] used a scaling function $F(r/\xi)$ in $g(r)$. The function $F(r/\xi)$ must allow for a breakdown of scaling of structure factor as a function of wave vector beyond a certain correlation length, i.e., $K<\xi^{-1}$. They used an exponential function for $F(r/\xi)$:

$$\begin{aligned}&F(r/\xi)\sim\exp(-r/\xi) ,\\&G(r)=\delta(r)+\frac{B}{r^{3-d_f}}\exp(-r/\xi) .\end{aligned} \tag{6}$$

Here, B is a constant.[21] Using this form of $G(r)$ gives the following expression for $S(K)$:

$$\begin{aligned}S(K)=1+\frac{C\Gamma(d_f-1)}{K}\xi^{d_f-1}(1+K^2\xi^2)^{(1-d_f)/2}\\\times\sin[(d_f-1)\arctan(K\xi)] ,\end{aligned} \tag{7}$$

where C is a constant and Γ is the gamma function. This expression redues to DK^{-d_f} for $K\xi\gg1$ and $Kr_0\ll1$, as it should, since then one probes length scales well within the fractal region. The expression is not valid for $Kr_0\geq1$ because the finite size of the monomers is not taken into account. Freltoft *et al.* were able to calculate an analytic expression for $S(K)$ in this case by assuming $g(r)=0$, $r\leq2r_0$.

For small particles (radius less than 100 nm, actually small values of Kr_0) the Guinier approximation for the form factor can be used: $P(K)=\exp(-K^2r_0^2/5)$, where r_0 is the optical radius of the particles. Substitution in Eq. (4) of this expression for the form factor and of Eq. (7) for the structure factor leads to

$$R(K)=\exp(-K^2r_0^2/5)\left[A_1+\frac{A_2}{K}\xi^{d_f-1}(1+K^2\xi^2)^{(1-d_f)/2}\sin[(d_f-1)\arctan(K\xi)]\right],$$

$$A_1=\kappa cM_m=R(K=0)\ \text{(monomers)},\quad A_2=\kappa cM_m C\Gamma(d_f-1)\ . \tag{8}$$

III. EXPERIMENT

The silica particles were synthesized according to Stöber's method[32] and coated with octadecyl alcohol following the procedure described by van Helden *et al.*[33] Experiments were done on three systems labeled SP23 (radius 24 nm), SJ9 (radius 31 nm), and SP45 (radius 33 nm). Characterization results for the particles dispersed in cyclohexane are given in Table I.

Silica particles were dried from dispersions in cyclohexane at 70 °C in a nitrogen flow. Weighted amounts of silica were dissolved in weighed amounts of solvent, i.e., *n*-dodecane, *n*-tetradecane, and *n*-hexadecane. Particle volume fractions could then be calculated. In Table II some physical constants for the solvents are given. Dispersions were filtered through millipore filters with a pore diameter of 1 μm to remove dust particles. Dispersions in *n*-tetradecane and *n*-hexadecane were filtered at 50 °C since their cloud points are near room temperature. All dispersions were kept in sealed tubes at 50 °C in order to prevent any aggregation prior to the experiments.

The scattered light intensity from the sample was measured with a Fica 50 photometer. We used the green mercury line, i.e., 546 nm wavelength. The scattering angles at which data were taken ranged from 15°–140° ($K\sim0.4\times10^7$ to 3×10^7 m^{-1}) usually at 5° intervals.

Temperature was measured in the toluene bath using a platinum resistance thermometer. The toluene bath was temperature controlled by a water flow from a thermostat (Julabo, ultratemp 2000) through a coil placed in the bath. Samples were allowed to equilibrate for temperature and aggregate size before data were taken. It was assumed that equilibration was complete when the scattering signal was constant. When the temperature was suddenly lowered to a few degrees below the cloud point, equilibration took about 10 min, after which the scattering signal remained constant for more than 1 day. Quench experiments in which the time dependence of the aggregate size was measured were done as follows. Temperature in the toluene bath was set at the quench temperature and allowed to equilibrate. Cuvettes were filled with samples taken from the tubes which were stored at 50 °C. Cuvettes were then put into the toluene bath of the Fica photometer which resulted in a temporary increase in temperature. The temperature was allowed to stabilize again; this took about 5 min. This point (after 5 min) was taken as the onset time for aggregation.

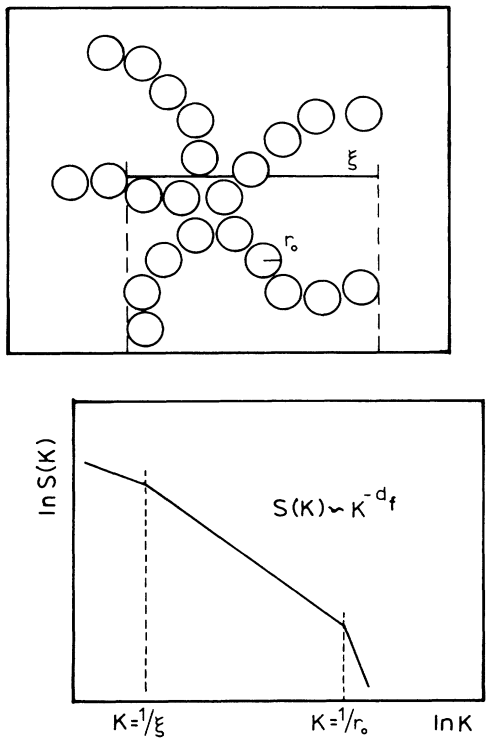

FIG. 1. Different K regions for structure factor of clusters.

IV. RESULTS AND DISCUSSION OF THE FRACTAL DIMENSION

A. Light scattering from system SP45 dispersed in *n*-dodecane

When cooling a dispersion of silica dispersed in *n*-dodecane from room temperature, both the hydrodynamic radius [determined from dynamic light scattering (DLS)] (Ref. 29) and the radius of gyration (determined from static light scattering) increase as the cloud point is approached. If the temperature is decreased below the cloud point the dispersion becomes very viscous and, if the temperature is lowered still further, a gel forms. Figure 2 shows a number of "Guinier" plots ($\ln[R(K)]$ versus K^2) as measured on SP45 dispersed in *n*-dodecane

TABLE I. Characterization results for silica particles dispersed in cyclohexane.

Colloidal system	SP23	SJ9	SP45
Electron microscopy			
r_{EM} (nm)	23.5	30.9	32.8
Standard deviation (nm)	2.3	4.0	4.2
Dynamic light scattering			
r_{HY} (nm)	32	38	41
Mass density			
ρ_d (g ml^{-1})	1.61	1.75	1.63

TABLE II. Physical constants for *n*-dodecane, *n*-tetradecane, and *n*-hexadecane.

	n-dodecane	*n*-tetradecane	*n*-hexadecane
Melting point (°C)	−9 to −10	6–8	17.5–18.5
Boiling point (°C)	215–216	252–254	287[b]
Density at 20 °C ($g\,ml^{-1}$)	0.748–0.749	0.762	0.772–0.774
Refractive index, n_d^{20}	1.4251[a]	1.429	1.434–1.435

[a] Wavelength equals 546 nm, temperature equals 25 °C (Ref. 35).
[b] See Ref. 36.

with a particle volume fraction of 0.012 at different temperatures using SLS. At temperatures below 16 °C the Guinier plot starts to curve steeply at small K. Usually this is ascribed to particle clusters in the sample and it is not possible to derive a characteristic particle size from the slope of the plot. Similar observations are made in DLS. Near 16 °C there is a large increase in the second cumulant. This cumulant gives the deviation of single exponential decay of the intensity auto correlation function. It goes to zero when only one time scale is present (monodisperse system).

In Fig. 3 we plot $\ln[R(K)]$ versus $\ln(K)$ for the same data as in Fig. 2. Power-law behavior of $R(K)$ and K is observed at low temperatures. The fractal dimension obtained from the plot at the lowest temperature is 2.08 ± 0.05. The error also includes uncertainty with regard to reproducibility. At higher temperatures the finite size of the clusters causes a leveling off of the scattering curves at low wave vectors. This also follows from Fig. 4 where we plotted measurements with smaller decrements in quench temperature. From many quench experiments (from room temperature to temperatures below the cloud point) on the SP45 in *n*-dodecane sample, we found that the fractal dimension varied nonsystematically between 1.98 and 2.08. These experiments also include some measurements where samples were quenched in an ice and water mixture after which light scattering was performed at 12 °C. This was the lowest temperature we could achieve without condensation forming on the glass of the toluene bath. The experimental values of d_f are close to the value found for chemically limited aggregation. The curves are similar in shape to the scattering curves obtained by Freltoft *et al.*

B. Different solvents

Dispersions of SJ9 in *n*-dodecane, *n*-tetradecane, and *n*-hexadecane with volume fraction 0.05 were quenched to about 10 °C below the cloud point (see Fig. 13 for cloud points). All samples showed gelation and the scattering curves $[\ln R(K)]$ versus $\ln(K)$ are shown in Fig. 5. The scattered light intensity for SJ9 samples in dodecane and tetradecane is very high at low angles. This is caused by the refractive-index difference between particles and solvent which increases in the order: *n*-hexadecane, *n*-tetradecane, and *n*-dodecane. In hexadecane the particles are almost index matched and scattered intensity is small. Data for dodecane and tetradecane shown in Fig. 5 have been corrected for double scattering (see Appendix B). The correction slightly changes the intensity levels but not the slope and thus d_f. Power-law behavior is observed in all three cases. The fractal dimension was determined from these curves using least-

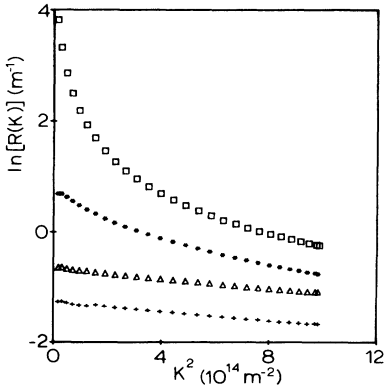

FIG. 2. Guinier plots for SP45 in *n*-dodecane at different temperatures. Volume fraction is 0.012. +, $T=20.7$ °C; △, $T=17.0$ °C; ∗, $T=15.8$ °C; □, $T=12.7$ °C. Curves are shifted along the Y axis, preserving the sequence in scattering intensities.

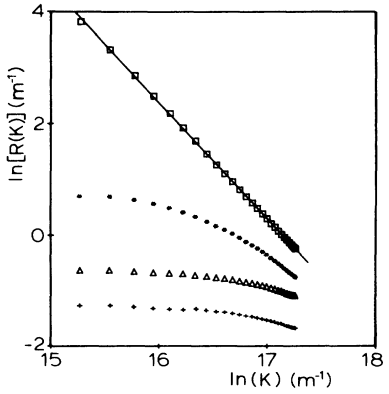

FIG. 3. Power-law scaling of scattering curves for SP45 in *n*-dodecane at different temperatures with large temperature decrements. Volume fraction is 0.012. +, $T=20.7$ °C; △, $T=17.0$ °C; ∗, $T=15.8$ °C; □, $T=12.7$ °C. The solid line has a slope 2.08. Curves are shifted along the Y axis, preserving the sequence in scattering intensities.

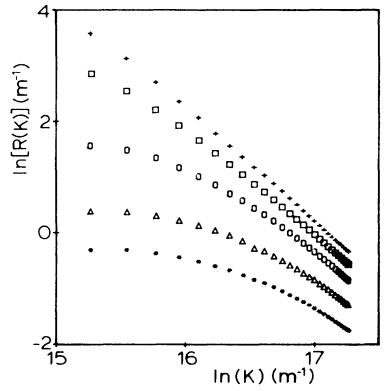

FIG. 4. Power-law scaling of scattering curves for SP45 in *n*-dodecane at different temperatures with small temperature decrements. Volume fraction is 0.012. *, $T=15.8\,^{\circ}C$; △, $T=15.5\,^{\circ}C$; ○, $T=15.0\,^{\circ}C$; □, $T=14.6\,^{\circ}C$; +, $T=14.1\,^{\circ}C$. Curves are shifted along the Y axis, preserving the sequence in scattering intensities.

squares methods. We find d_f(*n*-dodecane)$=2.07\pm0.05$, d_f(*n*-tetradecane)$=2.14\pm0.05$, and d_f(*n*-hexadecane) $=2.15\pm0.05$. The slight bending at low K in the SJ9-dodecane data makes it more difficult to determine the fractal dimension, but it is safe to say that the fractal dimensions for the three samples are the same within experimental error. These values for d_f again are close to the value found for chemically limited aggregation.

C. Influence of volume fraction

We studied the influence of particle volume fraction on aggregation by quenching samples of SP23 dispersed in *n*-dodecane to 11.6 °C, which is well below the cloud point of the dispersions. Four volume fractions were used: 0.01, 0.02, 0.03, and 0.05. The scattering curves are shown in Fig. 6. Data were taken at scattering angles $\geq 30^{\circ}$ and corrected for double scattering. The curves show power-law behavior, although the scattering curve for the highest concentration shows a slight bending. The fractal dimensions that were found from the curves are 2.17 ± 0.05 ($\phi=0.01$), 2.14 ± 0.05 ($\phi=0.02$), 2.11 ± 0.05 ($\phi=0.03$), and 1.99 ± 0.05 ($\phi=0.05$). In Fig. 7 we plot the values of d_f as a function of volume fraction. Although the value of d_f at the highest concentration may not be correct, it is seen from these data that fractal dimension tends to become smaller when volume fraction is increased.

D. Particle size

We can summarize the measurements in *n*-dodecane as follows. For SP45 with volume fraction equal to 0.012 we find $d_f=2.05\pm0.05$. The fractal dimension for the SJ9 sample with volume fraction 0.05 was 2.07 ± 0.05. From the experiments on SP23 in which we used volume fractions ranging from 0.01–0.05, a mean value for d_f can be deduced equal to 2.1 ± 0.1. It can thus be concluded that fractal dimension does not depend on particle radius. This conclusion may not be general, however, since we have only studied a limited particle size region. All measurements can be well described with $d_f=2.1\pm0.1$, which covers the range that is found in literature for chemically limited aggregation.

V. RESULTS AND DISCUSSION OF FRACTAL GROWTH EXPERIMENTS

It has been recognized that knowing the fractal dimension of a system does not enable one to identify the mechanism by which aggregates are formed. Before assuming that a particular mechanism is involved one should also study aggregation kinetics. An exception can be made for aggregation processes based on the Smoluchowski equation, for which good quantitative descriptions exist

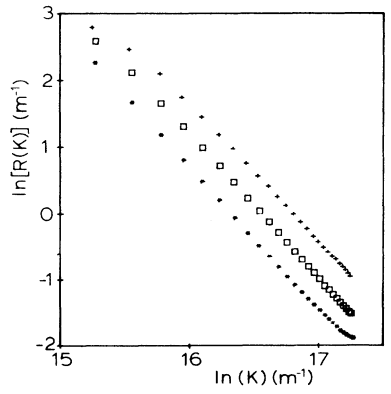

FIG. 5. Influence of solvent: scattering curves for SJ9 in different alkanes with volume fraction equal to 0.05. *n*-dodecane (+), *n*-tetradecane (□), *n*-hexadecane (*). Samples were quenched well below the cloud point. Curves are shifted along the Y axis, preserving the sequence in scattering intensities.

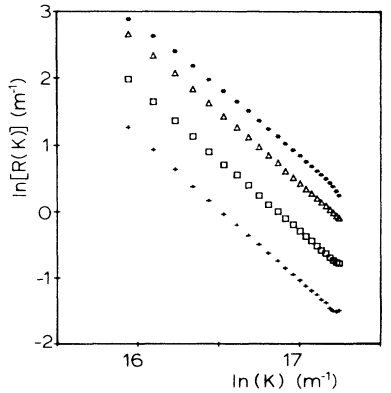

FIG. 6. Influence of volume fraction: scattering curves for SP23 in *n*-dodecane at 11.6 °C. Volume fraction 0.01 (+), 0.02 (□), 0.03 (△), and 0.05 (*). Curves are shifted along the Y axis, preserving the sequence in scattering intensities.

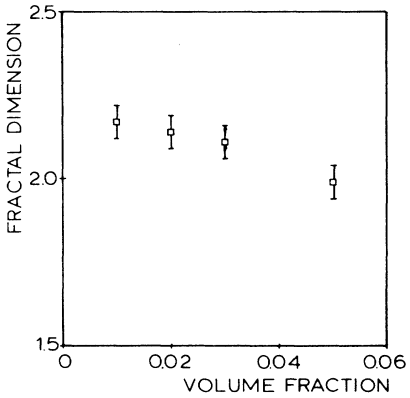

FIG. 7. Fractal dimension as a function of volume fraction for SP23 in n-dodecane. Samples were quenched to 11.6 °C.

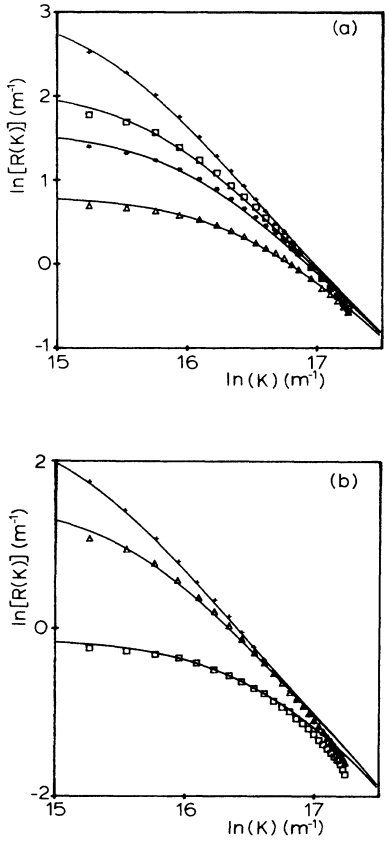

FIG. 8. (a) Growth kinetics: scattering curves for SP23 in n-dodecane as a function of time during aggregation at 16.3 °C. Volume fraction is 0.02. Solid curves are fits using a finite cluster radius and $d_f=2.1$. △, $t=146$ min, $\xi=61$ nm; *, $t=416.2$ min, $\xi=93$ nm; □, $t=663.2$ min, $\xi=120$ nm; +, $t=1461.2$ min, $\xi=198$ nm). (b) Growth kinetics: scattering curves for SP45 in n-dodecane as a function of time during aggregation at 15.2 °C. Volume fraction is 0.012. Solid curves are fits using a finite cluster radius and $d_f=2.1$. □, $t=30$ min, $\xi=62$ nm; △, $t=90$ min, $\xi=150$ nm; +, $t=150$ min, $\xi=243$ nm.

that give unique relations between kinetics and structure.[34] As described in the Introduction, each mechanism implies a specific relation between aggregate radius and time. Combination of the fractal dimension and kinetics by which the fractal is formed can help one to decide which growth mechanism is appropriate for the experiments at hand. In Sec. IV we found $d_f=2.1\pm0.1$; in this section we study the cluster growth.

Aggregation of SP23 dispersed in n-dodecane ($\phi=0.02$) was studied at 16.3 °C. At this temperature aggregation is slow since it is only ~ 1 °C below the cloud point. Scattering curves were measured as a function of time during one day. Temperature remained constant to well within 0.1 °C. Corrected scattering curves (see Appendix B) are shown in Fig. 8(a). We analyzed the scattering curves using the expression for $R(K)$ given in the theory section, assuming that clusters with fractal dimension 2.1 are formed and that during aggregation only the size of the clusters changes. The value 2.1 is an average value obtained from the experiments described above. The size of the monomers r_0 was determined from a Guinier plot at 25 °C. From this experiment we found $r_0=34.7$ nm, $R(K=0)=0.562$ m^{-1}. The value for $R(K=0)$ was corrected for the temperature dependence of the refractive index of the dispersion to find $R(K=0)$ for the monomers at 16.3 °C. This value equals A_1 and was found to be 0.379 m^{-1}. In Eq. (8) we also need A_2, which is found as follows. For $\xi^{-1}<K<r_0^{-1}$, Eq. (8) can be approximated by

$$R(K)=\exp(-K^2r_0^2/5)(A_1+A_2K^{-d_f}) .$$

By choosing $\ln(K)=16.6$ ($K=1.62\times10^7$ m^{-1}) we find the (constant) value of $A_2=2.4\times10^{15}$ m$^{-3.1}$. With these values for r_0, d_f, A_1, and A_2, we fitted the scattering curves using Eq. (8) and taking ξ as an adjustable parameter. The calculated curves describe the data very well, as can be seen from Fig. 8(a). It should be emphasized that for one particular system all scattering curves can be described with a cluster radius ξ, which is a function of time. Small deviations occur at high wave vectors, since here length scales near the order of the monomer size are probed and the expression for $R(K)$ is no longer valid. This explanation is supported by the observation that at high-wave-vector scattering data are the same at all aggregation times. Calculated curves are quite sensitive to the value of ξ, especially for small values of this parameter. This is illustrated in Fig. 9, where we have plotted two calculated curves and the scattering data at $t=341.2$ mins. ξ_1 is 76 nm and ξ_2 is 80 nm. It was found that, in general, ξ could be determined within 1 nm. In Fig. 10(a) we plotted cluster radius ξ as a function of aggregation time. The plot is linear throughout the time region which indicates that aggregation kinetics is linear with time.

Aggregation kinetics of SP45 in n-dodecane ($\phi=0.012$) was studied at 15.2 °C in the same way. Again we used a fractal dimension equal to 2.1. We found $r_0=45$ nm, $A_1=0.195$ m^{-1}, and $A_2=8.5\times10^{14}$ m$^{-3.1}$. Figure 8(b) shows calculated and experimental scattering curves. The calculated scattering curves de-

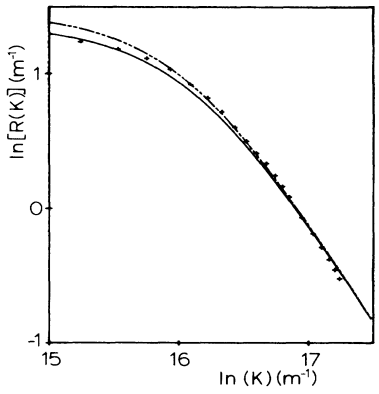

FIG. 9. +, scattering data for SP23 in *n*-dodecane for a quench at 16.3 °C. $t = 341.2$ min. Solid curve is calculated using $\xi = 80$ nm; dashed curve is calculated using $\xi = 76$ nm.

scribe the data rather well. Small deviations occur at high K values where the data are systematically below the theoretical curves. This is again due to the fact that at these high K values length scales of the order of the monomer size are probed and the expression for $R(K)$ no longer holds. As can be seen from Fig. 10(b), we again find a linear dependence of aggregate radius on time. It is thus found that aggregation kinetics is linear for both SP23 in *n*-dodecane and SP45 in *n*-dodecane. Aggregation can be described for both systems in terms of a growing fractal cluster with $d_f = 2.1$, the radius of which increases linearly with time. We think that this indicates that cluster growth proceeds via the chemically limited mechanism.

In theoretical work, relations between the mean cluster size $s(t)$ and time are used.[34] In the nongelling region one obtains $s(t) \sim t^z$. Since $s(t) \sim \xi^{d_f}$, for our experiments we find that $z = 2.1$.

Figure 11 shows a plot of cluster radius as a function of time for aggregation of octadecyl-coated silica dispersed in *n*-dodecane at three temperatures. It is emphasized that aggregation is faster at lower temperatures, which cannot readily be explained with a diffusion-limited process. From the slope of the curves in Fig. 11 a reaction constant k is calculated defined by

$$k = \frac{d\xi}{dt}\phi^{-1} .$$

We plot $\ln(k)$ versus $1/T$ (Arrhenius plot) in Fig. 12. From the slope the "transition enthalpy" is calculated: $\Delta H \sim -1800$ kJ mol^{-1}. Hence the reaction proceeds with a high exothermic enthalpy change. Such a behavior is typical for a process involving a "freezing" transition. We, therefore, suppose that this enthalpy change is caused by a "solidlike" or "nematiclike" ordering of either chains on the surface of the particles or solvent molecules in "necks" between the particles. The enthalpy of melting of hexadecane is -50 kJ mol^{-1}. This implies that per particle about 40 chains or solvent molecules are freezing or undergo a nematic ordering. When the overlap volume is calculated from $V_{\text{overlap}} = \pi\Delta^2\sigma/4$, then about 16 chains per two particles are involved. The cross-sectional area of their overlap volume is $\pi\Delta\sigma/2$.

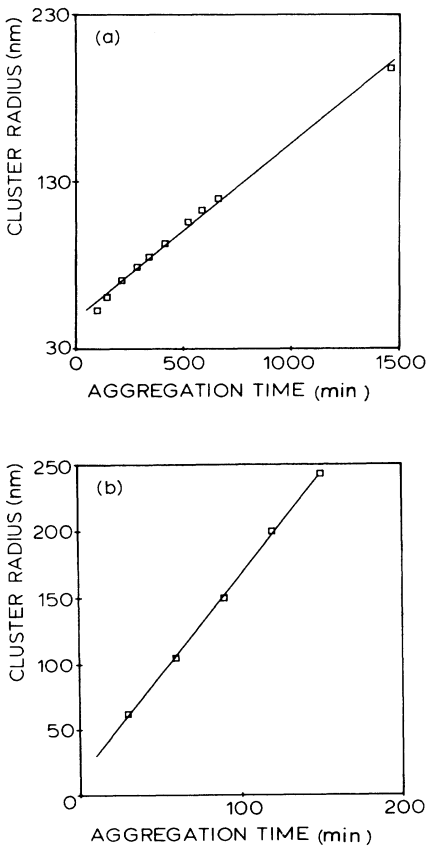

FIG. 10. (a) Cluster radius as a function of time for aggregation of SP23 in *n*-dodecane at 16.3 °C. Volume fraction is 0.02. (b) Cluster radius as a function of time for aggregation of SP45 in *n*-dodecane at 15.2 °C. Volume fraction is 0.012.

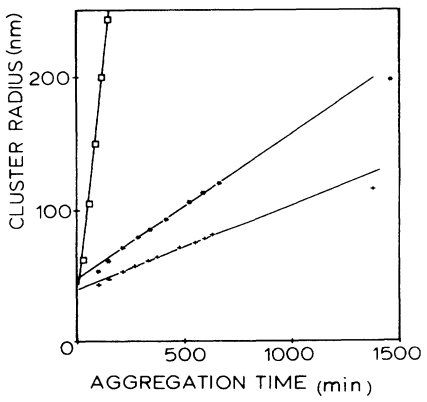

FIG. 11. Cluster radius as a function of time: +, SP23 in *n*-dodecane, $\phi = 0.02$, $T = 16.6$ °C; *, SP23 in *n*-dodecane, $\phi = 0.02$, $T = 16.3$ °C; □, SP45 in *n*-dodecane, $\phi = 0.012$, $T = 15.2$ °C.

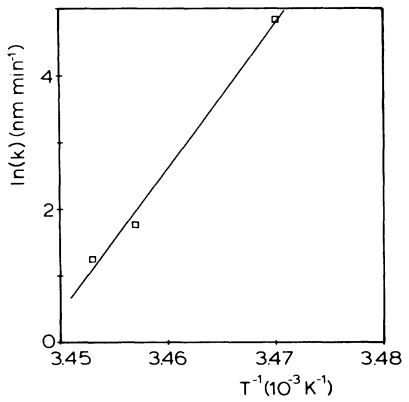

FIG. 12. Arrhenius plot for aggregation of octadecyl silica dispersed in *n*-dodecane.

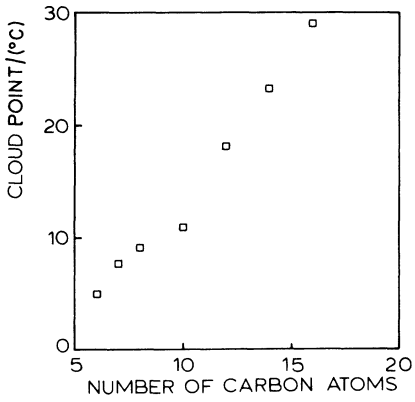

FIG. 13. Cloud point as a function of carbon number for dispersions of SJ9 in *n*-alkanes. Volume fraction is 0.05.

Each chain or solvent molecule has a cross-sectional area of 20–30 Å^2. Therefore, in this case, about 170 molecules are involved. The experimentally calculated value is in between these limits. Although this reflection is by no means beyond any doubt, it nevertheless explains the order of magnitude we find for ΔH.

VI. CONCLUSION

The aggregation of sterically stabilized silica particles dispersed in linear alkanes can be described by a chemically limited cluster aggregation model. Using the description of Freltoft *et al.* our experiments can be described satisfactorily in terms of a fractal cluster dimension of 2.1 ± 0.1 and a linear growth of the clusters with time. For the exponent z in the relation between mean fractal size and time, we find a value of 2.1. The observed growth kinetics suggests nematic ordering of the stabilizing chains or solvent molecules upon contact of two particles.

Since aggregation in these systems is reversible, we systematically probed the influence of alkane solvent, particle volume fraction, particle size, and quench depth. None of these parameters, except the volume fraction, has a systematic influence on the results. The fractal dimension seems to decrease with increasing volume fraction.

ACKNOWLEDGMENTS

The authors wish to thank Professor A. Vrij and Professor M. H. Ernst for stimulating discussion and criticism. S. M. McNab is thanked for making some linguistic and stylistic improvements.

APPENDIX A

In Fig. 13 we plotted the cloud point (the temperature at which phase transition occurs) as a function of the number of carbon atoms in the *n*-alkane solvent for silica particles with radius 31 nm (code SJ9). Cloud points were determined by measurement of the turbidity of the dispersions as a function of temperature.[28] The volume fraction of particles was 5%. All dispersions show phase separation upon cooling. Dispersions in alkanes with carbon number ≤ 10 showed phase transition in two fluid phases with different particle concentration. Dispersions in alkanes with carbon number ≥ 12 showed gelation.

APPENDIX B

Here, we briefly discuss the influence of multiple scattering on the scattering curves. Since scattered intensity at low K values can become very large [$R(K) > 10$ m^{-1}] multiple scattering may influence the scattering data. On the basis of his calculations on multiple scattering[37,38] Dhont has written a computer program that uses an iterative correction procedure to correct scattering data for double scattering. To use the program, $R(K=0)$ has to be known; this is usually obtained by extrapolation of $R(K)$ against K^2. Since our Guinier plots are very steep for small K, this extrapolation is difficult. However, it turned out that correction for double scatter-

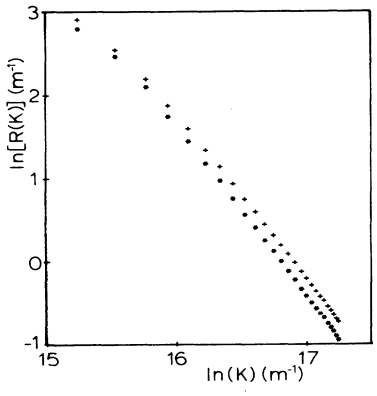

FIG. 14. Influence of double scattering on scattering data of SJ9 in *n*-dodecane, volume fraction is 0.05, temperature is 14 °C. +, data before correction; *, data after correction.

ing was not very sensitive to the precise value of $R(K=0)$. Therefore, although the values of $R(K=0)$ may not be very accurate, the corrections are reliable. In Fig. 14 we show two sets of data taken on SJ9 in *n*-dodecane ($\phi=0.05$) at 14 °C: one is before correction the other is after correction. From this figure we see that correction essentially shifts the data to lower values of $\ln[R(K)]$ and affects the K dependence of $R(K)$ only to a minor degree. We corrected the scattering data for SP45 in *n*-dodecane at 12.7 °C and found $d_f=2.10$, which is the same value as found before correction. In the analyses of scattering curves in terms of finite aggregate size, we always used corrected data.

APPENDIX C

Martin and Ackerson[31] have shown that the fractal dimension as determined by light scattering may not be the correct value. This fractal dimension is influenced by power-law polydispersity, i.e., $N(R)\sim R^{-\tau}$. They found the following relations:

$$R(K)\sim\begin{cases}K^{-d_f(3-\tau)}, & \tau>2\\ K^{-d_f}, & \tau<2\ .\end{cases}$$

Especially in the case of gelation where τ is known to be larger than 2 there is a large effect of polydispersity on the power-law behavior of $R(K)$ and K. Then the fractal dimension as measured by light scattering is smaller than the actual fractal dimension of the clusters. In the nongelation region τ is smaller than 2 and polydispersity of the clusters does not affect the fractal dimension. From the experiments presented here, we cannot conclude that there is a significant difference between the gelation and the nongelation region. Fractal dimensions as determined in both regions are the same. The decrease in d_f with increasing ϕ for the quench experiments on SP23 in *n*-dodecane can, however, be explained by an increase in polydispersity. The viscosity of the samples increases for higher volume fractions and the sample with $\phi=0.05$ formed a gel. This may indicate that τ increases with volume fraction, which in turn may lead to lower apparent fractal dimensions.

[1]B. B. Mandelbrot, *The Fractal Geometry of Nature* (Freeman, New York, 1982).

[2]D. A. Weitz and J. S. Huang, in *Kinetics of Aggregation and Gelation,* edited by F. Family and D. P. Landau (Elsevier, Amsterdam, 1984), pp. 19–28.

[3]T. A. Witten and L. M. Sander, Phys. Rev. Lett. **47**, 1400 (1981).

[4]P. Meakin, Phys. Rev. Lett. **51**, 1119 (1983).

[5]M. Kolb, R. Botet, and R. Jullien, Phys. Rev. Lett. **51**, 1123 (1983).

[6]M. Kolb and R. Jullien, J. Phys. (Paris) Lett. **45**, 977 (1984).

[7]P. Meakin, in *On Growth and Form,* edited by H. E. Stanly and N. Ostrowsky (Martinus-Nijhof, Boston, 1986), pp. 111–135.

[8]P. Meakin, Annu. Rev. Phys. Chem. **39**, 237 (1988).

[9]S. K. Sinha, T. Freltoft, and J. Kjems, in Ref. 2, pp. 87–90.

[10]D. A. Weitz and M. Oliveria, Phys. Rev. Lett. **52**, 1433 (1984).

[11]C. Aubert and D. S. Cannell, Phys. Rev. Lett. **56**, 738 (1986).

[12]M. Kolb, Phys. Rev. Lett. **53**, 1653 (1984).

[13]D. W. Schaefer, J. E. Martin, P. Wiltzius, and D. S. Cannell, Phys. Rev. Lett. **52**, 2371 (1984).

[14]R. C. Ball, D. A. Weitz, T. A. Witten, and F. Leyvraz, Phys. Rev. Lett. **58**, 274 (1987).

[15]D. A. Weitz, J. S. Huang, M. Y. Lin, and J. Sung, Phys. Rev. Lett. **54**, 1416 (1985).

[16]D. S. Cannell and C. Aubert, in Ref. 7, pp. 187–197.

[17]P. Meakin and R. Jullien, J. Phys. (Paris) **46**, 1543 (1985).

[18]R. Botet, R. Jullien, and M. Kolb, in *Fractals in Physics,* edited by L. Pietronero and E. Tosatti (Elsevier, Amsterdam, 1986), pp. 255–258.

[19]M. Kolb, in Ref. 18, pp. 263–266.

[20]D. W. Schaefer and K. D. Keefer, in Ref. 18, pp. 39–45.

[21]T. Freltoft, J. K. Kjems, and S. K. Sinha, Phys. Rev. B **33**, 269 (1986).

[22]J. E. Martin and A. J. Hurd, J. Appl. Crystallogr. **20**, 61 (1987).

[23]D. S. Horne, Faraday Spec. Discuss. Chem. Soc. **83**, 259 (1987).

[24]P. N. Pusey and J. G. Rarity, Mol. Phys. **62**, 411 (1987).

[25]J. E. Martin, Phys. Rev. A **36**, 3415 (1987).

[26]P. W. Rouw, A. Vrij, and C. G. de Kruif, Colloids Surf. **31**, 299 (1988).

[27]J. Edwards, D. H. Everett, T. O'Sullivan, I. Pangalon, and B. Vincent, J. Chem. Soc. Faraday Trans. I **80**, 2599 (1984).

[28]J. W. Jansen, C. G. de Kruif, and A. Vrij, J. Colloid Interface Sci. **114**, 481 (1987).

[29]P. W. Rouw, A. Vrij, and C. G. de Kruif, Progr. Colloid Polym. Sci. **76**, 1 (1988).

[30]P. A. Egelstaff, *An Introduction to the Liquid State* (Academic, London, 1967), pp. 91–105.

[31]J. E. Martin and B. J. Ackerson, Phys. Rev. A **31**, 1180 (1985).

[32]W. Stöber, A. Fink, and E. Bohn, J. Colloid Interface Sci. **26**, 62 (1968).

[33]A. K. van Helden, J. W. Jansen, and A. Vrij, J. Colloid Interface Sci. **81**, 354 (1981).

[34]M. H. Ernst, in Ref. 18, pp. 289–302.

[35]M. B. Huglin, *Light Scattering From Polymer Solutions* (Academic, London, 1972), p. 29.

[36]*Handbook of Chemistry and Physics,* 55th ed. (Chemical Rubber Company, Cleveland, 1974).

[37]J. K. G. Dhont, Physica A **120**, 238 (1983).

[38]J. K. G. Dhont, C. G. de Kruif, and A. Vrij, J. Colloid Interface Sci. **105**, 539 (1985).